

## Ecosystem carbon and water cycling from a sky island montane forest

John F. Knowles<sup>a,b,\*</sup>, Russell L. Scott<sup>a</sup>, Rebecca L. Minor<sup>b</sup>, Greg A. Barron-Gafford<sup>b</sup>

<sup>a</sup> Southwest Watershed Research Center, USDA-ARS, Tucson, AZ, United States

<sup>b</sup> University of Arizona, Tucson, AZ, United States



### ARTICLE INFO

#### Keywords:

Monsoon  
Flux  
Productivity  
CO<sub>2</sub>  
Evapotranspiration  
Arizona

### ABSTRACT

“Sky islands” are characteristic of sequential mountain-valley terrain where mountains form an island archipelago rising from surrounding valleys of desert “sea”. At high elevations in the Madrean sky islands of the southwestern United States (USA) and Mexico, mixed evergreen conifer forests occur near the latitudinal extent of their distribution. This setting provides a unique opportunity to explore the ecosystem response to warmer and drier conditions that are forecasted to become more common throughout the species range. Accordingly, this work used the eddy covariance method to quantify carbon and water cycling dynamics from a Madrean sky island forest ecosystem for nine years between 2009 and 2018. The forest functioned as net sink of carbon dioxide throughout the year, which resulted in more carbon sequestration than other monitored montane forests in the continental western USA. Sustained forest activity was made possible by the combination of mild winter temperatures and a bimodal precipitation regime that delivered moisture during both summer and winter. Seasonally, gross primary production (*GPP*) was temperature limited in winter and could become moisture limited during the dry early summer period depending on antecedent snowmelt moisture. Ecosystem respiration was more sensitive than *GPP* to moisture availability throughout the rest of the non-winter period. Forecasted warming could thus stimulate forest carbon gains during the winter and either increase or decrease respiratory carbon loss during summer as a function of moisture. Overall, a metric of snow aridity that included snow depth and potential evapotranspiration was the best predictor of the warm season carbon balance ( $R^2 = 0.86$ ). The seasonally dissimilar impacts of warming and drying identified by this work inform current understanding of how climate change and/or variability may affect forest water and carbon cycling dynamics throughout the montane forest biome.

### 1. Introduction

Mountain forests are responsible for the majority of sustained carbon sequestration in the semiarid western USA (Schimel et al., 2002; Desai et al., 2011). However, these ecosystems may be increasingly vulnerable to disturbance as a result of climate change (Dale et al., 2001; Williams et al., 2010). In particular, increasing drought is forecasted for this area, and forest carbon uptake is already seasonally moisture limited in many places (Seager et al., 2007; Knowles et al., 2018). The potential consequences of drought in semiarid regions are especially severe, and have been linked to widespread vegetation mortality and reductions in the global carbon balance (Ahlstrom et al., 2015; Breshears et al., 2005). For these reasons, it is essential to understand the carbon cycling dynamics of mountain forest ecosystems across the full range of hydrometeorological and species composition gradients on the landscape.

The North American Monsoon (monsoon) describes an atmospheric

pattern that results in convective thunderstorm activity that peaks in July and August and concludes the highly arid pre-summer period (pre-monsoon) across the southwestern USA and northwestern Mexico (Adams and Comrie, 1997; Higgins et al., 1999). Since the relative importance of monsoon precipitation is dependent on latitude, this produces a north-south gradient in the ratio of winter to summer precipitation throughout the region (Douglas et al., 1993). Previous work has shown that monsoon precipitation can be critically important for rescuing individual trees from winter drought (Peltier and Ogle, 2019), but the relative impact of summer precipitation on the annual montane forest carbon cycle is a currently open ecohydrological question (Berkelhammer et al., 2017; Hu et al., 2010; Szejner et al., 2016). Further, changes in the seasonal timing and the magnitude of monsoon precipitation may occur with climate change (Cook and Seager, 2013; Pascale et al., 2019), with implications for the seasonality of drought and forest production. As a result, montane forests in the southwestern USA provide a unique opportunity to constrain the impact of

\* Corresponding author at: USDA-ARS Southwest Watershed Research Center, 2000 E. Allen Road, Tucson, AZ 85719, United States.

E-mail address: [john.knowles@usda.gov](mailto:john.knowles@usda.gov) (J.F. Knowles).

<https://doi.org/10.1016/j.agrformet.2019.107835>

Received 11 July 2019; Received in revised form 17 October 2019; Accepted 8 November 2019

Available online 20 November 2019

0168-1923/ Published by Elsevier B.V.

precipitation seasonality on growing season moisture availability and subsequent ecosystem carbon and water fluxes.

Forest production is commonly assumed to be limited by growing season length in evergreen conifer forests (Churkina et al., 2005; Piao et al., 2007). However, recent work has shown that this may not be the case in some Mediterranean-climate montane forest ecosystems where winters are mild and production can occur year-round (Barnard et al., 2018; Kelly and Goulden, 2016). Monsoon-affected “sky island” forests occur in areas of continental mountain-valley terrain, where vegetation communities stack vertically to encompass a range of ecosystems usually distributed across broad latitudinal gradients, and represent a potentially similar but understudied ecosystem due to inherently remote and complex terrain. The Madrean archipelago spans a globally unique temperate-to-tropical climatic gradient and contains approximately 40 sky islands between southern Arizona and New Mexico, USA and northwestern Mexico (Warshall, 1995). Madrean sky island forests are warmer than higher latitude continental forests, but also more arid due to persistent subtropical high atmospheric pressure. There is broad consensus that a lengthened dry season and increased plant water demand will accompany increased aridification that is forecasted for the southwestern USA (Archer and Predick, 2008; Seager et al., 2007); hence, the degree to which current temperature versus moisture or other factors limit production from sky island forests could inform the trajectory of more northerly continental forests under climate change. The results of this scenario will have significant implications for the current and future western USA carbon sink (Schwalm et al., 2012).

The overarching goal of this study was to evaluate the seasonal ecohydrological dynamics of a sky island montane forest that may serve as a proxy for future conditions along the Rocky Mountain cordillera. To address this, we leveraged nine years of continuous eddy covariance data from the Santa Catalina Mountains, Arizona, USA that included periods of distinct hydrometeorological variability. The specific objectives of this work were to: (1) characterize baseline patterns of evergreen conifer forest carbon and water cycling variability near the latitudinal extent of a species distribution, and to (2) evaluate the relative importance of seasonal meteorology, principally including monsoon precipitation, to ecosystem dynamics. We hypothesized that mild winters and the reliable influx of monsoon precipitation during the summer would combine to relax seasonal moisture and temperature limitations to growth relative to higher latitude and/or lower elevation sites.

## 2. Materials and methods

### 2.1. Study site

The study was located on the western slope of Mt. Bigelow (32°25′00″ N; 110°43′31″ W; 2753 m above sea level) in the Santa Catalina Mountains, approximately 29 km northeast of Tucson, Arizona, USA (Brown-Mitic et al., 2007) (Fig. 1). Topographically, the site is situated on a broad ridge near the top of a north-south oriented saddle with a generalized slope of 11% (Brown-Mitic et al., 2007). The second-growth mixed evergreen conifer forest is predominantly composed of ponderosa pine (*Pinus ponderosa*), Douglas-fir (*Pseudotsuga menziesii*), and southwestern white pine (*Pinus strobiformis*) with a mean canopy height of 10 m and no significant understory vegetation. Tree ring analysis indicates forest re-establishment after logging in the 1930s (Potts et al., 2017). The two-dimensional statistical measurement footprint of the eddy covariance measurements (Kljun et al., 2015) was consistently omnidirectional, with an elongation to the southwest along the prevailing wind direction (237°) (Fig. 1a). Footprint maps did not indicate significant deviations between years or seasons. Generally, on an annual basis, ~50% of flux originated from within ~150 m upwind and 80% of flux originated from within ~500 m upwind. Within 150 m of the 30-meter tall tower, the forest ranged from 47 to 87 percent tree cover, with areas of greater cover to south and west and less cover to

the north and east (Fig. 1b). In 2012, portions of forest near the instrument tower were selectively thinned to promote horizontal and vertical diversity in the form of more dense forest stands spaced farther apart. This treatment was generally restricted to south-facing slopes to the southeast of the tower; hence, away from the zone of peak measurement sensitivity. Qualitative analysis indicates that ~30% of the forest was thinned in these areas. The soil texture is sandy loam with 32% sand, 41% silt, and 26% clay and a pH of 5.4 (Sánchez-Cañete et al., 2018). Depth to bedrock is 1 m or less.

The 1965–1980 (longest available record) mean annual precipitation (PPT) and air temperature ( $T_{air}$ ) were 790 mm (including snow) and 9.3 °C, respectively, at the Palisades Ranger Station, approximately 340 m below and 1.2 km southeast of the study site. The region experiences a semiarid climate and is subject to both the effects of the North American Monsoon and the El Niño-Southern Oscillation (ENSO; Adams and Comrie, 1997; Brown-Mitic et al., 2007). This results in distinct summer and winter precipitation maxima separated by a pronounced dry season. For the current study, we defined five seasons according to the following classification: winter (November to February), spring (March and April), pre-monsoon (May and June), monsoon (July and August), and fall (September and October). During the winter, snow is common, but a seasonally-continuous snowpack does not always develop. In its absence, ephemeral snow cover can accumulate and ablate many times in one season. Recognizing the effect of winter precipitation on ensuing warm season ecosystem dynamics, the water year (WY) was defined as the period from 1 November to 31 October.

### 2.2. Instrumentation and measurements

An eddy covariance system was used to quantify the surface-atmosphere exchange of heat, water vapor, and carbon dioxide (CO<sub>2</sub>) between 1 November 2009 and 31 October 2018 (AmeriFlux site code US-MtB). Turbulent fluxes were calculated as the 30-minute covariances between 10 Hz deviations in vertical wind speed and air temperature or gas density using a co-located three-dimensional sonic anemometer (CSAT 3, Campbell Scientific, Logan, UT, USA) and an open path infrared gas analyzer (IRGA) (LI-7500; Li-Cor, Lincoln, NE, USA) mounted at 29.8 m above ground level (agl) and oriented to the northwest at 290°. Radiation was measured by a four-component radiometer (CNR1; Kipp & Zonen, Delft, Netherlands) and a net radiometer (NR-Lite; Kipp & Zonen, Delft, Netherlands), both mounted at 16 m agl facing south. South-facing air temperature and humidity sensors were mounted at 1.5 m, 16 m, and 31 m agl prior to 19 September 2013 (shielded HMP45C; Vaisala, Helsinki, Finland), and at 1.5 m, 8.75 m, 16 m, 24 m, and 31 m agl thereafter (shielded HMP60; Vaisala, Helsinki, Finland). Unless otherwise noted, air temperature and humidity data from the lowest measurement height are reported. Potential evapotranspiration was calculated on a daily basis following the Penman approach (Shuttleworth, 1993).

Precipitation was measured at three tipping bucket gages (TR-525 M or TR-525USW; Texas Electronics, Dallas, TX, USA): one located at 29 m near the top of the tower (“top”), one ~2 m south of the tower (“bottom”), and one 30 m north of the tower in a forest canopy gap (“gap”). Each winter, either the bottom or gap gage was fitted with a snow adapter (CS705; Campbell Scientific, Logan, UT, USA), and the measurement from that gage was used during precipitation events that occurred when air temperature was below 5 °C. When air temperature was above 5 °C, and when precipitation was detected by the top gage, the largest volume of precipitation recorded by any of the gages was used, in order to reduce the potential impacts of wind-induced undercatch and canopy interception. After 1 January 2018, precipitation recorded at the Sollers RAWS (Remote Automatic Weather Station) site (approximately 380 m below and 1.9 km to the southeast of Mt. Bigelow) was used due to malfunctions in both the bottom and gap gages. Between 2010 and 2017, the mean annual precipitation at the

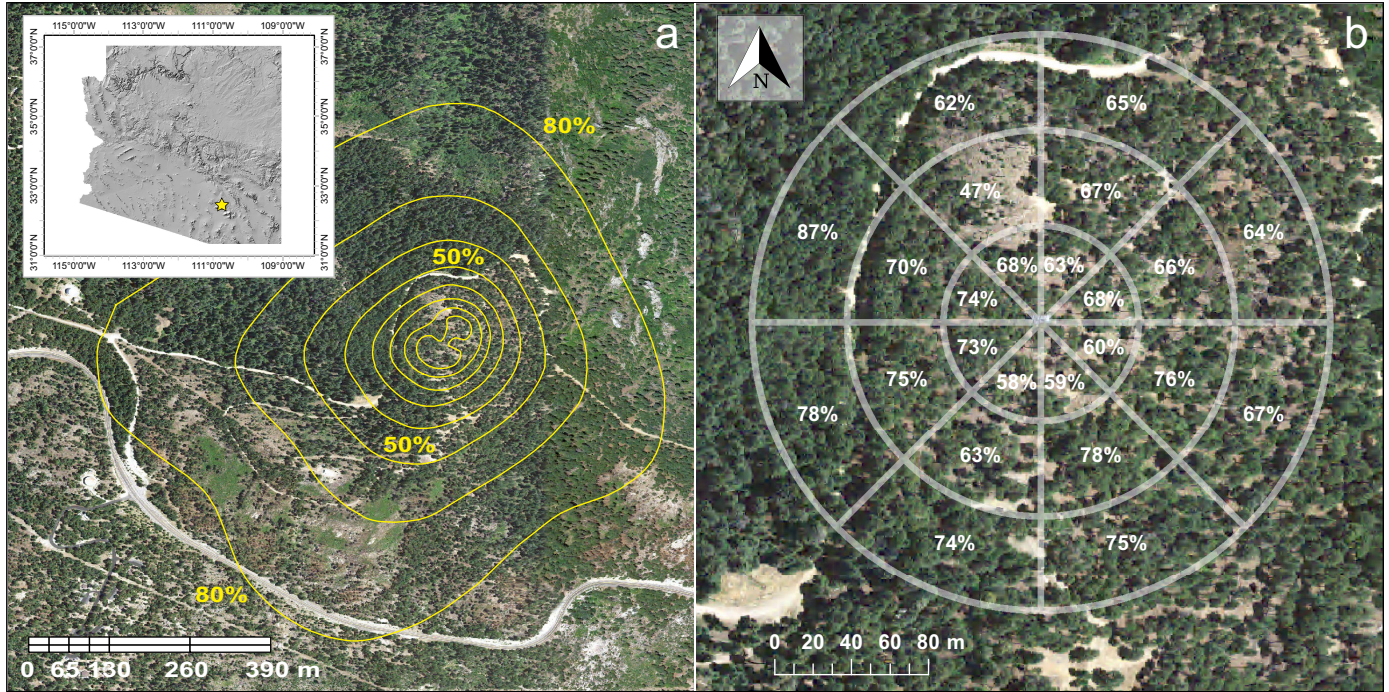


**Fig. 1.** The Mt. Bigelow study site. (a) Two-dimensional representation of the source area contributing to turbulent flux measurements between 1 January 2017 and 31 December 2017. Yellow contours denote cumulative percent contributions in 10% increments with the 50% and 80% contours labeled for reference. (b) Spatial distribution of vegetation cover within 300 horizontal meters of the instrument tower. Inset hillshade map shows the location of Mt. Bigelow (yellow star) in the Madrean sky island province of Arizona, USA. Background images © National Agriculture Imagery Program.

Sollers gage was 579 mm (605 mm at Mt. Bigelow), and the total annual Sollers precipitation and the Mt. Bigelow precipitation were significantly correlated ( $R^2 = 0.58$ ;  $p = 0.03$ ) in these years. Seasonal correlation between the Sollers and Mt. Bigelow precipitation records was highest during the pre-monsoon and monsoon periods ( $R^2 = 0.82$ ;  $p < 0.001$ ) and lowest during the spring ( $R^2 = 0.13$ ), potentially due to precipitation phase differences resulting from the elevation difference between sites. Snow depth was measured as the average of two ultrasonic depth sensors (Judd Communications, Salt Lake City, UT, USA) located on approximately flat terrain at a distance of 30 m from the tower.

Soil temperature was characterized from profile measurements at three locations near the eddy covariance tower. Soil temperature sensors (handmade Type E thermocouples) were buried to depths of 0 cm, 2 cm, 4 cm, 8 cm, 16 cm, 32 cm, and 64 cm below the soil surface. Here we report results from 4 cm depth (composite data from 4 cm probes at all three pits) as a balance between surface and deeper soil conditions. Soil heat flux was calculated as the average of six soil heat flux plates (HFP01-L; Hukseflux, Delft, Netherlands) buried 5 cm beneath the soil surface and corrected for the change in heat storage between them and the surface. Data were sampled at 10 Hz (sonic anemometer and infrared gas analyzer) or 1 s (all other sensors) and averaged to 30-minute means by a datalogger (CR5000, CR1000, or CR10X; Campbell Scientific, Logan, UT, USA). All instruments were powered by solar panels via a battery bank.

### 2.3. Data processing

Data quality assurance requires special attention in mountainous terrain (e.g., Stiperski and Rotach, 2016). Post processing of the eddy covariance data included two dimensional coordinate rotation and the addition of terms to account for density fluctuations as documented below (Lee, 2004; Webb et al., 1980). An additional inferred heat term,  $S_{op}$ , was derived to account for potential bias of the open path IRGA due to heating of the instrument body (Burba et al., 2008):

$$S_{op} = \frac{F_C^{cp} - \overline{w'\rho_c'} - \mu \left( \frac{\rho_c}{\rho_d} \right) \overline{w'\rho_v'}}{\rho_c \left[ 1 + \mu \left( \frac{\rho_v}{\rho_d} \right) \right]} T_{air} - S \quad (1)$$

where  $F_C^{cp}$  is the CO<sub>2</sub> flux ( $\text{mg m}^{-2} \text{s}^{-1}$ ) measured by the sonic anemometer and a closed path IRGA (LI-7200, Li-Cor, Lincoln, NE, USA) using closed path gas mixing ratios that are not subject to sensor heating effects (Burba et al., 2012),  $\overline{w'\rho_c'}$  is the open path covariance between vertical wind speed and CO<sub>2</sub> density ( $\text{mg m}^{-2} \text{s}^{-1}$ ),  $\mu$  is the ratio of the molecular mass of air to water,  $\rho_c$  is the mean ambient CO<sub>2</sub> density ( $\text{mg m}^{-3}$ ),  $\rho_d$  is the mean dry air density ( $\text{mg m}^{-3}$ ),  $\rho_v$  is the mean water vapor density ( $\text{mg m}^{-3}$ ),  $\overline{w'\rho_v'}$  is the open path covariance between vertical wind speed and water vapor density ( $\text{mg m}^{-2} \text{s}^{-1}$ ),  $T_{air}$  is air temperature (K), and  $S$  is the sensible heat flux ( $\text{K m s}^{-1}$ ). The  $S_{op}$  term was calculated and averages were derived separately for daytime (incoming solar radiation  $\geq 10 \text{ W m}^{-2}$ ) and nighttime (incoming solar radiation  $< 10 \text{ W m}^{-2}$ ) conditions from three years of simultaneous open path and closed path data collection between 1 January 2014 and 31 December 2016. The resultant values were applied to the entire open path dataset by:

$$F_C^{sop} = \overline{w'\rho_c'} + \mu \left( \frac{\rho_c}{\rho_d} \right) \overline{w'\rho_v'} + \left( 1 + \mu \frac{\rho_v}{\rho_d} \right) (S + S_{op}) \left( \frac{\rho_c}{T_{air}} \right) \quad (2)$$

where  $F_C^{sop}$  is open path CO<sub>2</sub> flux corrected for sensor heating. This procedure was necessary to produce a full-length record of CO<sub>2</sub> exchange given that the closed path gas analyzer was not deployed to the site until late 2013, and its time series was less complete than the open path IRGA after deployment. Attempts to model  $S_{op}$  based on temperature, sensible heat flux, and solar radiation independently did not result in better agreement with closed path fluxes relative to the use of daytime and nighttime averages.

Both the  $S_{op}$  correction and a similar, established sensor-heating correction (Burba et al., 2008) resulted in significantly less carbon uptake than the uncorrected flux, particularly during the daytime, indicating that sensor self-heating was affecting data quality from the

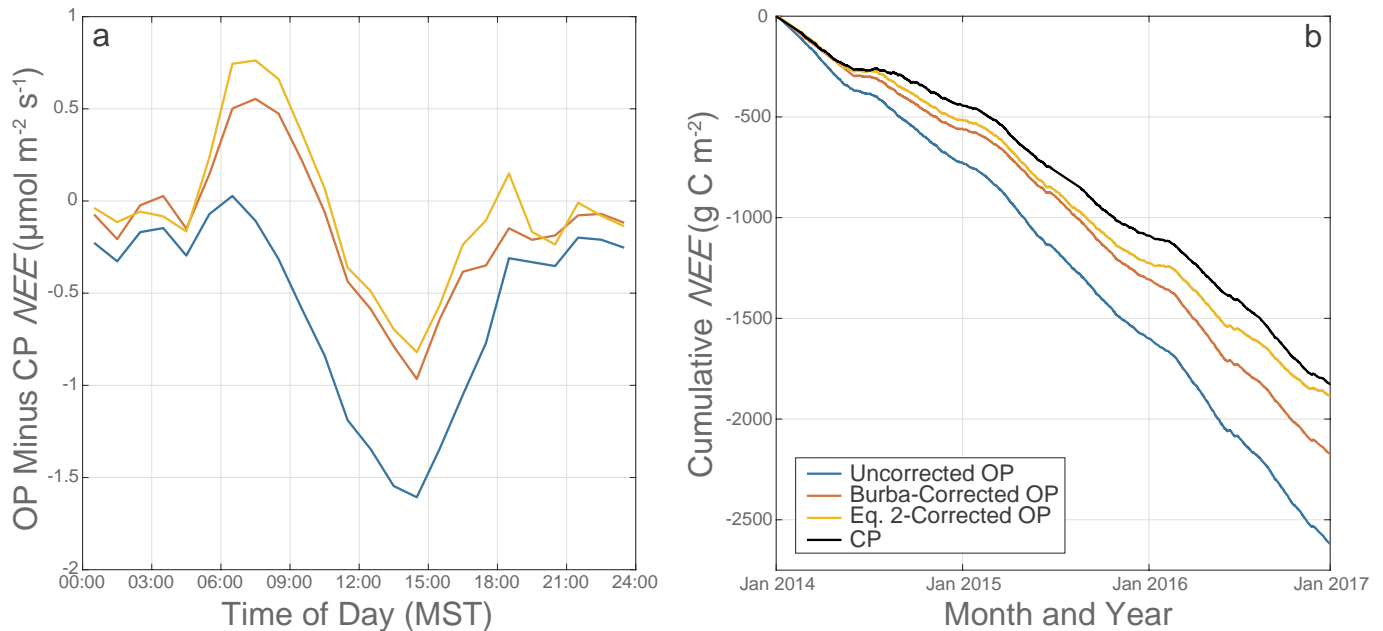


**Fig. 2.** The effect of the  $S_{op}$  Correction to the open path gas analyzer. (a) The average difference between the closed path  $NEE$  and the uncorrected, Burba-corrected, and  $S_{op}$ -corrected open path  $NEE$  throughout the day. (b) The cumulative effect of the Burba and  $S_{op}$  corrections over time relative to the uncorrected open path (OP) and closed path (CP) fluxes. Each panel represents unfiltered (for turbulent mixing) data from 1 January 2014 through 31 December 2016.

open path sensor (Fig. 2). Although neither correction resulted in perfect agreement with the closed path flux at all periods throughout the day, the summed daily difference between the open and closed path fluxes was reduced from  $-0.60 \text{ mg CO}_2 \text{ m}^{-2}$  (uncorrected) to  $-0.16 \text{ mg CO}_2 \text{ m}^{-2}$  (Burba) or  $-0.06 \text{ mg CO}_2 \text{ m}^{-2}$  ( $S_{op}$ ). Over three years of simultaneous data collection, the Burba correction reduced the cumulative net ecosystem exchange of  $\text{CO}_2$  ( $NEE$ ) by  $452 \text{ g C m}^{-2}$ , whereas the  $S_{op}$  correction reduced the cumulative  $NEE$  by  $748 \text{ g C m}^{-2}$  to within 3% of the closed path flux during the same period (Fig. 2b).

#### 2.4. Measurement uncertainty and gapfilling

Uncertainty in eddy covariance data includes myriad random and systematic sources of error (Goulden et al., 1996). Whereas random errors tend to cancel out when averaged over periods of years or more, the effect of systematic errors resultant from data collection or processing methods can be compounded over time (Lasslop et al., 2010). Notwithstanding, many systematic errors can also be remedied through calibration. Energy balance closure, or the degree to which radiative fluxes of net radiation ( $R_n$ ) and soil heat ( $G$ ) are balanced by turbulent fluxes of latent ( $LE$ ) and sensible ( $H$ ) heat, corresponds to the influence of systematic error on eddy covariance data through conservation of energy. Given that stable atmospheric conditions can negatively impact energy balance closure, particularly in areas of complex terrain where insufficient turbulent mixing can result in beneath-sensor advective flows (Turnipseed et al., 2002), we compared friction velocity ( $u^*$ ), an indicator of turbulent mixing, to energy balance closure across a range of environmental conditions (Fig. 3).

The 30-minute mean energy balance closure at Mt. Bigelow was 0.77 in summer (combined pre-monsoon and monsoon), 0.62 in winter, and averaged 0.74. These values were comparable to a synthesis of 22 eddy covariance sites across a range of ecosystem and climate types (Wilson et al., 2002), and may reflect the general inability of point measurements to capture large-scale atmospheric motion under particular circumstances (Foken, 2008; De Roo et al., 2018). In general, energy balance closure was proportional to friction velocity up to a threshold value ( $0.45 \text{ m s}^{-1} < u^* < 0.55 \text{ m s}^{-1}$ ) and then gradually declined thereafter. In order to balance data inclusion and quality, a

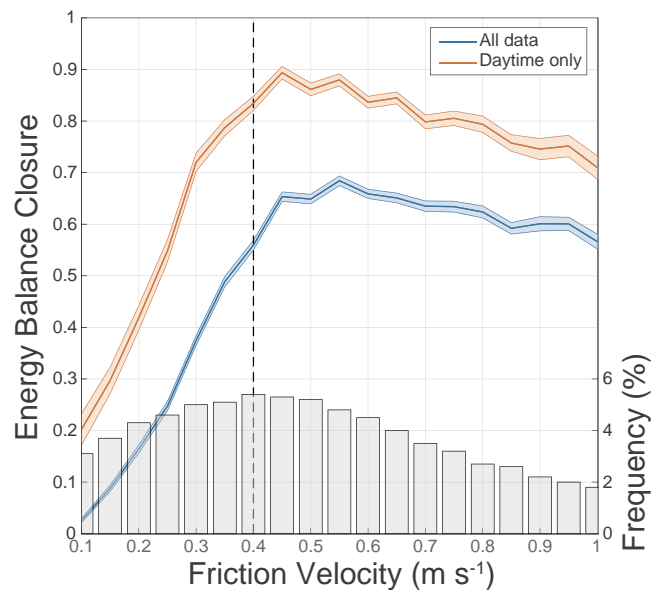


**Fig. 3.** Energy balance closure as a function of binned (bin size =  $0.05 \text{ m s}^{-1}$ ) friction velocity. Dashed line shows the friction velocity cutoff ( $0.4 \text{ m s}^{-1}$ ) that was applied before the gapfilling process. Bars correspond to the histogram of observed friction velocities (all data).

friction velocity cutoff of  $0.4 \text{ m s}^{-1}$  was applied to the complete dataset. Data were additionally excluded when the wind direction originated from between  $105^\circ$  and  $115^\circ$ , in order to reduce potential interference from the anemometer mount. After further removal of obviously bad data, 51% of the 30-minute data were included in the final analysis. In spite of this rigorous procedure, we acknowledge the potential for significant uncertainty to affect the data reported herein, especially due to the influence of drainage flows in complex terrain (Novick et al., 2014; Turnipseed et al., 2002), and we emphasize our use of annual sums as comparative, rather than absolute, measures with which to evaluate inter-annual shifts in ecosystem function (Baldocchi, 2008;

Lasslop et al., 2010).

All micrometeorological and flux data were gapfilled using the REddyProc algorithm version 1.1.6 (Wutzler et al., 2018). At this stage, the *NEE* data were additionally partitioned into constituent gross primary productivity (*GPP*) and ecosystem respiration (*R<sub>eco</sub>*) fluxes using a light-response curve approach (Lasslop et al., 2010). This method was selected in favor of nighttime-based methods due to the prevalence of low *u\** conditions during the night. We followed the micrometeorological sign convention where positive *NEE* corresponds to flux directed away from the surface (source) and negative *NEE* corresponds to flux directed toward the surface (sink). The *GPP* and *R<sub>eco</sub>* fluxes are always greater than or equal to zero. The continuous, gapfilled data were used to derive long-term plots and sums for the purpose of comparison; all other analyses were performed using non-gapfilled data.

### 3. Results and discussion

#### 3.1. Site hydroclimatology

Mt. Bigelow has a bimodal annual precipitation distribution, typical of the Madrean sky island province, with abundant rainfall in the summer and cool and more variably wet winters (Fig. 4). Significant hydrometeorological variability during the winter (Nov – Feb) resulted

from the passage of frontal systems associated with snow accumulation and periods of below-freezing air temperatures. In between these systems, winter daytime air temperatures commonly exceeded 10 °C or more, and the average winter air temperature was 3.7 °C. The lowest recorded air temperature was –23 °C on 3 February 2011. Spring was a transition period in terms of air temperature and precipitation, which could occur in the form of rain or snow. The pre-monsoon (May – Jun) was the driest time of year from both an atmospheric (vapor pressure deficit; *VPD*) and hydrologic (*PPT*) perspective, and both monthly maximum (23.1 °C) and minimum (14.6 °C) air temperature peaked in June, as well as mean *VPD* (1.6 kPa). The highest recorded air temperature was 33.9 °C on 27 June 2012. The monsoon (Jul – Aug) had the highest precipitation amounts and persistently warm conditions. On average, 47% and 25% of annual precipitation occurred during the monsoon and winter seasons, respectively. Precipitation was lower during the fall (Sep – Oct) and could result from either an extended monsoon period or occasional but intense extratropical cyclones.

The sky island hydroclimatic regime at Mt. Bigelow showed similarities and differences to both deserts and montane forests throughout the western USA. Although Mt. Bigelow was cooler and wetter than the surrounding desert, we observed a similar bimodal monsoon precipitation distribution with a peak during the monsoon. However, the accumulation of a seasonal snowpack resulted in a reliable and delayed

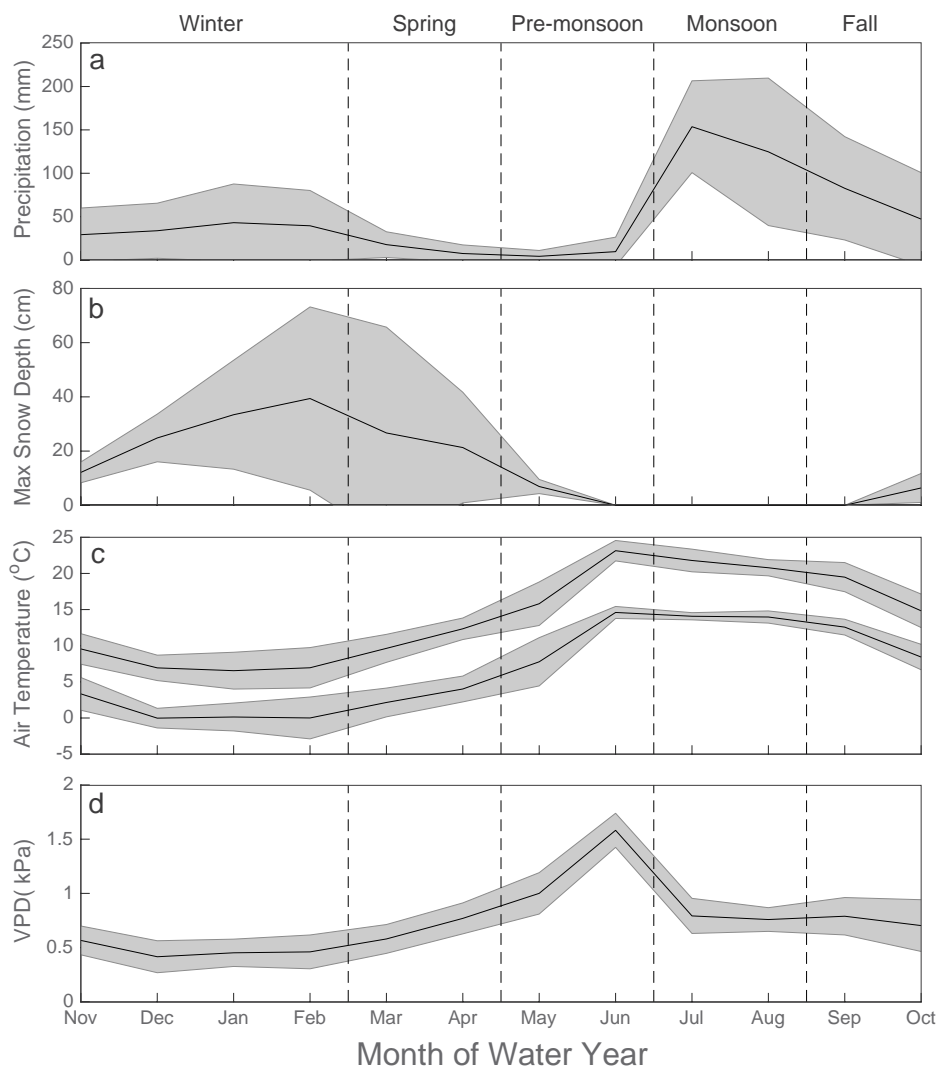


Fig. 4. The seasonal climatology between water years 2010 and 2017 (snow depth) or 2018 (all other variables). Solid lines show monthly mean values and shaded areas denote one standard deviation. Both mean monthly maximum and minimum air temperatures are included in (c). *VPD* is vapor pressure deficit.

**Table 1**

Meteorological conditions and ecohydrological fluxes by water year (1 November – 31 October). The  $T_{\text{air}}$  is the annual mean, Snow Depth is the annual maximum, and all other variables are gapfilled annual sums. Negative  $NEE$  corresponds to net  $\text{CO}_2$  uptake by the surface. Note the flux partitioning algorithm does not force the  $GPP$  and  $R_{\text{eco}}$  to sum to  $NEE$ .

| Water Year | $T_{\text{air}}$ (°C) | PPT (mm) | Snow Depth (cm) | ET (mm) | NEE ( $\text{g C m}^{-2}$ ) | GPP ( $\text{g C m}^{-2}$ ) | $R_{\text{eco}}$ ( $\text{g C m}^{-2}$ ) |
|------------|-----------------------|----------|-----------------|---------|-----------------------------|-----------------------------|------------------------------------------|
| 2010       | 9.0                   | 618      | 123             | 708     | -549                        | 1284                        | 780                                      |
| 2011       | 9.7                   | 342      | 36              | 599     | -503                        | 1221                        | 739                                      |
| 2012       | 10.7                  | 616      | 36              | 730     | -603                        | 1316                        | 1010                                     |
| 2013       | 9.5                   | 571      | 39              | 707     | -507                        | 1062                        | 639                                      |
| 2014       | 10.4                  | 638      | 17              | 665     | -371                        | 1058                        | 696                                      |
| 2015       | 9.7                   | 666      | 25              | 855     | -492                        | 1249                        | 825                                      |
| 2016       | 9.8                   | 826      | 66              | 865     | -582                        | 1252                        | 670                                      |
| 2017       | 10.3                  | 620      | 56              | 806     | -534                        | 1204                        | 723                                      |
| 2018       | 10.9                  | 627      | -               | 761     | -651                        | 1269                        | 700                                      |
| Mean       | 10.0                  | 614      | 50              | 744     | -532                        | 1213                        | 754                                      |
| SD         | 0.6                   | 125      | 33              | 87      | 80                          | 93                          | 111                                      |

Abbreviations:  $T_{\text{air}}$ , air temperature; PPT, precipitation; ET, evapotranspiration;  $NEE$ , net ecosystem exchange; GPP, gross primary productivity;  $R_{\text{eco}}$ , ecosystem respiration.

secondary moisture pulse that is not common at lower elevations (Warshall, 1995). Compared to other montane forest ecosystems in the western USA, Mt. Bigelow was generally warmer and drier, with seasonally dissimilar precipitation due to its location on the northward edge of the core monsoon region in northwestern Mexico (Adams and Comrie, 1997). The monsoon precipitation maximum at Mt. Bigelow contrasts the winter precipitation maximum observed at coastal and higher latitude continental sites (Leung et al., 2003), which results in a diminished snowmelt moisture pulse, but also potentially less ecohydrological dependence on snowmelt moisture that is broadly declining throughout the western USA (Mote et al., 2018; Udall and Overpeck, 2017). In fact, two significant opportunities for precipitation annually (both winter and monsoon) could ultimately buffer Madrean sky islands from inter-annual ENSO variability or warm snow drought in the future (Cayan et al., 1999; Dierauer et al., 2019).

Between WY 2010 and WY 2018, the mean annual air temperature was 10.0 °C and the mean annual precipitation was 614 mm (Table 1). The nine-year study period was thus 0.7 °C warmer and 176 mm drier than the long-term (1965–1980) average, in accord with observed and forecasted drought in the southwestern USA (Cook et al., 2015; Woodhouse et al., 2010). Seasonally, the mean monsoon PPT was 289 mm (standard deviation (SD) = 95 mm). Monsoon PPT was significantly ( $> 1$  SD) above average in 2012 (389 mm) and 2016 (404 mm), and below average in 2011 (117 mm) and 2018 (183 mm). During the winter, mean PPT was 151 mm (SD = 60 mm); winter PPT was significantly above average in WY 2010 (229 mm) and WY 2017 (262 mm), and below average in WY 2011 (79 mm). Compounded winter and summer PPT deficits in 2011 resulted in an annual precipitation (342 mm) that was more than two standard deviations below the nine-year mean. The yearly maximum snow depth was highly variable and ranged from 17 cm in 2014 to 123 cm in 2010 (Table 1). The mean maximum snow depth was 50 cm.

The mean annual ET was 744 mm and resulted in an ET/PPT ratio of 1.25 (SD = 0.21) (Table 1). Given that precipitation undercatch is common in complex terrain and during periods of snow precipitation (Chubb et al., 2015), the true ET/PPT ratio at Mt. Bigelow is likely closer to unity. However, even considering undercatch, plant-accessible water storage likely supports ET through seasonal, and even possibly multi-year, dry periods (Rungee et al., 2018). For example, despite a significant water deficit, the 2011 GPP (1% above) and NEE (6% below) were close to the nine-year mean. The aridity index (PET/PPT) averaged 3.06 (SD = 0.95) on an annual basis, which indicates moisture limitation to ET, but less than is commonly observed (aridity index = 5

to 8) at lower elevations (Novick et al., 2016). Compared to the adjacent grassland and shrubland ecosystems, mean annual  $T_{\text{air}}$  at Mt. Bigelow was 7–9 °C lower, and precipitation was approximately double and similarly distributed throughout the year, albeit with no snow at lower elevations (Scott et al., 2015). Despite the predominance of the ET hydrological pathway, high-elevation catchments in this area are thus proportionally cool and wet, and contribute to significant mountain block recharge (Ajami et al., 2011; Thomas et al., 2016)

### 3.2. Carbon fluxes

Mt. Bigelow was a greater annual carbon sink ( $NEE = -532 \text{ g C m}^{-2}$ ) than other monitored montane forest locations in Arizona (US-FUF;  $NEE = -112 \text{ g C m}^{-2}$ ; Dore et al., 2012), Colorado (US-NR1;  $NEE = -217 \text{ g C m}^{-2}$ ; Knowles et al., 2015), and New Mexico, USA (US-VCM;  $NEE = -326 \text{ g C m}^{-2}$ ; Biederman et al., 2017). Notably, mean annual  $T_{\text{air}}$  was lower (1.3 to 8.7 °C) at these other sites, and the minimum annual  $NEE$  (largest carbon sink) at Mt. Bigelow coincided with the warmest year (Table 1). In terms of GPP, Mt. Bigelow was comparable to a Mediterranean-climate montane forest site (AmeriFlux site US-CZ3;  $GPP \approx 1250 \text{ g C m}^{-2}$ ; Kelly and Goulden, 2016) in California, USA (gapfilled  $NEE$  not reported from that site), with a similar mean annual  $T_{\text{air}}$  (9 °C). Both GPP and  $R_{\text{eco}}$  peaked in 2012, which was a warm year with above average precipitation, especially during the monsoon, that followed prolonged drought conditions during 2011 (Table 1). As a result, we interpret the 2012  $R_{\text{eco}}$  maximum within the context of previous work suggesting that the magnitude of the post-drought  $R_{\text{eco}}$  pulse upon soil rewetting is proportional to the length and severity of the antecedent dry period (Birch, 1958; Noy-Meir, 1973). This phenomenon has been characterized across a range of semiarid sites including sky islands and deserts (Barron-Gafford et al., 2011; Hamerlynck et al., 2013; Olshansky et al., 2019; Scott et al., 2010, 2009), and potential causes include drought-induced changes in hydrological connectivity (Smith et al., 2017), bacterial growth (Meisner et al., 2015), and/or substrate availability (Ma et al., 2012).

### 3.3. Seasonal dynamics

We observed distinct seasonal patterns in the diurnal meteorological cycles and fluxes (Fig. 5). For example, daytime high temperatures were comparable in the monsoon and pre-monsoon seasons, but nighttime low  $T_{\text{air}}$  typically remained above 15 °C during the monsoon. In contrast, nighttime  $T_{\text{air}}$  could drop below 12 °C during the pre-monsoon (Fig. 5a), reflecting increased net longwave cooling (data not shown) due to the relatively clear, dry atmospheric conditions during this time. The 7 °C diurnal temperature range during the pre-monsoon was the largest of any season. The average nighttime winter air temperature remained above freezing at 2.8 °C. The VPD was significantly higher during the pre-monsoon compared to any other season (Fig. 5b). The LE peaked during the monsoon with the co-occurrence of elevated available energy and moisture (Fig. 5c). The  $NEE$  was most negative during the spring and fall as a consequence of the spring  $R_{\text{eco}}$  minimum and the fall GPP maximum (Fig. 5d–f). Leaf-level measures of tree function have shown a similar peak in net photosynthetic rates during the fall (Potts et al., 2017). A strong diurnal GPP cycle was maintained throughout the year, including during winter when the flux was still approximately 50% of warm season rates. The diurnal  $R_{\text{eco}}$  cycle was sharply curtailed during the winter.

In contrast to the prevailing notion of winter dormancy for montane evergreen forest ecosystems (Biederman et al., 2017; Bourdeau, 1959; Havranek and Tranquillini, 1995), we observed significant GPP throughout the year (Fig. 6b). Winter specifically accounted for 19% of total annual GPP despite a mean daytime high temperature of only 6 °C (Fig. 5). This level of wintertime activity was comparable to the US-CZ3 Mediterranean-climate forest where the mean daytime high temperature was 5.1 °C and winter GPP was 17% of total annual GPP (Kelly and

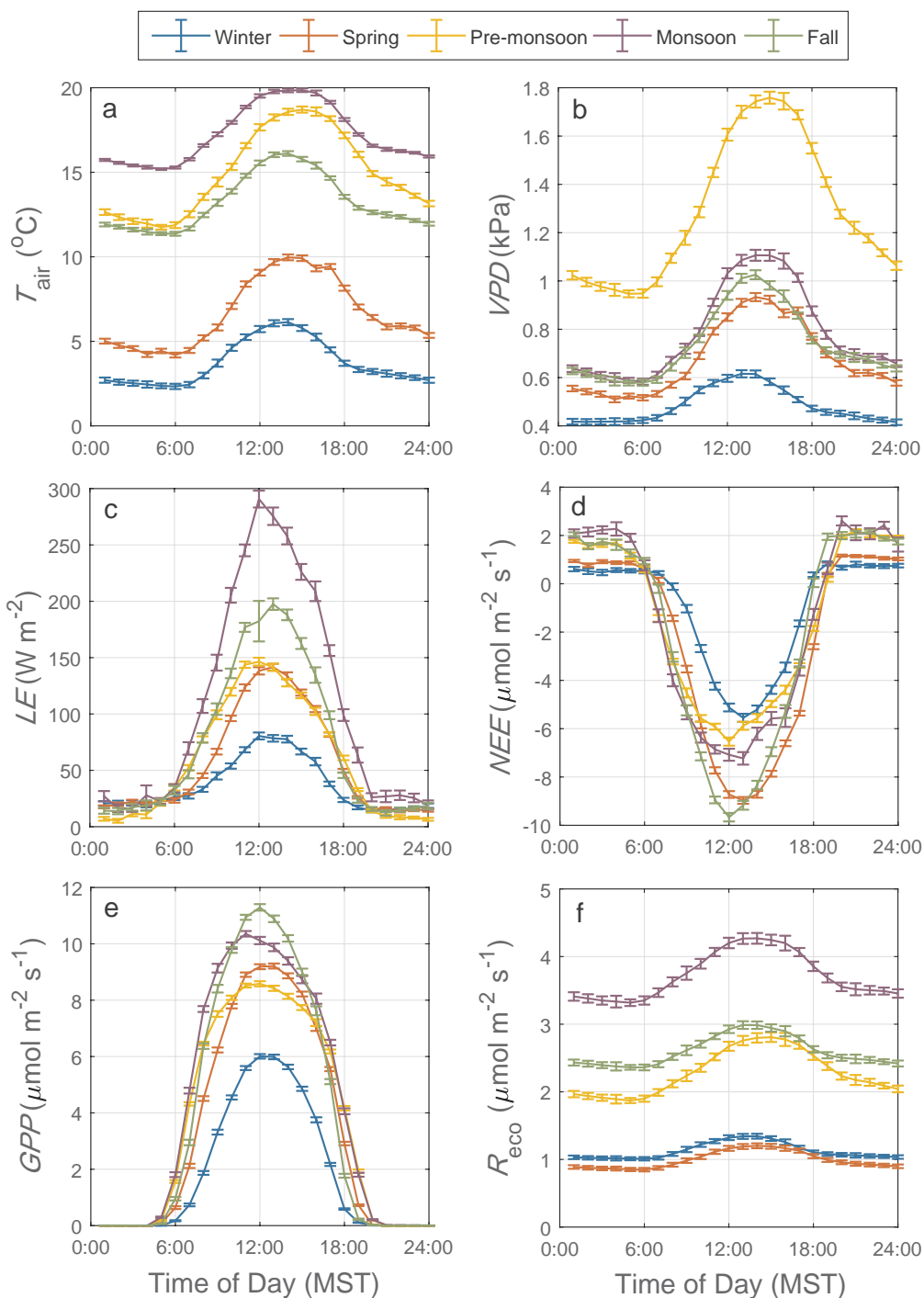
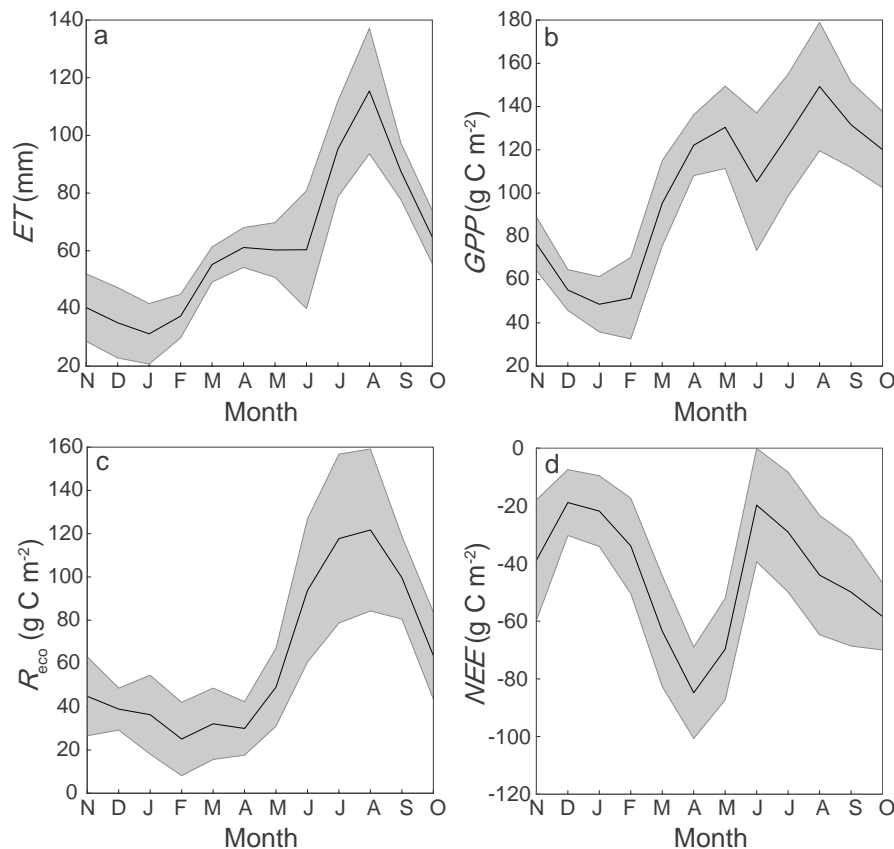


Fig. 5. Mean diurnal cycles of select meteorological and ecohydrological variables by season. Bars denote the standard error.

Goulden, 2016). During the spring,  $GPP$  ramped up faster than  $R_{eco}$ , which remained relatively low until June (Fig. 6c). It has been suggested that forecasted earlier snowmelt could reduce the carbon sink strength of colder evergreen conifer forests with negligible winter activity by increasing the temporal disconnect between favorable moisture and temperature conditions during the critical spring snowmelt period to tree growth (e.g. Winchell et al., 2016). Here, a warmer climatology is superimposed onto that scenario to show that potential low temperature-limitation to early spring  $GPP$  as a result of earlier snowmelt may be alleviated in the presence of winter warming (Huxman et al., 2003). Consequently,  $R_{eco}$  continues to lag  $GPP$ , thus preserving the spring carbon use efficiency ( $CUE$ ;  $-NEE/GPP$ )

maximum, albeit shifted earlier in the season, in accord with lower elevation systems in the southwestern USA (e.g. Biederman et al., 2018).

Seasonal asynchrony between  $GPP$  and  $R_{eco}$  resulted in a bimodal  $NEE$  distribution where the forest functioned as a stronger carbon sink during the spring and fall and a weaker carbon sink during the summer (combined pre-monsoon and monsoon) (Fig. 6d). Overall, the magnitude of  $R_{eco}$  dominated the seasonal  $CUE$  signal (e.g., Valentini et al., 2000), which peaked at 68% following the spring snowmelt pulse and was lowest during the pre-monsoon (38%) and monsoon (26%) periods. Despite maximum water use efficiency ( $GPP/ET$ ) during the climatologically dry pre-monsoon period, we interpret reductions in both  $GPP$  and



**Fig. 6.** The seasonal evolution of water and carbon fluxes throughout the water year. Solid lines show monthly mean values and shaded areas denote one standard deviation.

NEE during the month of June as evidence of moisture limitation to vegetation (Fig. 6). Notwithstanding, a disparity between the pre-monsoon GPP (higher) and  $R_{\text{eco}}$  (lower) suggests that reduced moisture availability affects  $R_{\text{eco}}$  more than GPP, which parallels the model of riparian desert systems (Scott et al., 2014) and seasonally dry rainforests where carbon uptake is greater during the dry season (Saleska et al., 2003), as long as there is sufficient subsurface hydrologic carryover from the previous wet season (Guan et al., 2015). From a hydrological perspective, these results imply that a forecasted prolonged pre-monsoon period could decrease GPP until the onset of monsoon precipitation, but that longer or more frequent dry periods disproportionately inhibit  $R_{\text{eco}}$  and thereby increase the ecosystem carbon sink strength during the remainder of the warm season when moisture is not generally limiting to vegetation.

### 3.4. Inter-annual variability

Seasonal precipitation and evaporation fluxes shared a common summer maximum and were more closely aligned in time than snow precipitation-dominated mountain systems in the western USA (Bales et al., 2006) (Fig. 7a). However, the relative magnitudes of the winter and monsoon precipitation maxima were highly variable on an inter-annual basis (Fig. 7a). The ratio of winter to monsoon precipitation ranged from 30% in 2012 to 84% in 2017 and averaged 56%. The warm and dry pre-monsoon conditions sometimes extended back into the spring, and there was always a period of at least 75 days with less than 25 mm cumulative precipitation before the first summer rains. Dry conditions in 2011 resulted from the driest monsoon and the second driest winter, spring, and pre-monsoon seasons in our record. This translated to the lowest ET of all nine years. During the wettest year (2016), precipitation was average up to and through the pre-monsoon,

which was followed by extremely wet monsoon and fall periods. Correspondingly, the 2016 ET was the highest of any year, although the inter-annual variability of the ET flux was generally damped relative to precipitation (Fig. 7b). We determined significant positive relationships between precipitation and ET for all groupings of seasons (not shown) and years (Fig. 7c).

The forest was a relatively steady carbon sink in some years, while other years were punctuated by periods of weak or negligible carbon uptake lasting between weeks and months (Fig. 8a). Diminished carbon uptake was primarily restricted to periods of low temperatures during the winter or dry conditions during the pre-monsoon that could persist into the following season depending on severity. The ecosystem generally functioned at near-maximum carbon sink strength between March and May and again between August and October. Exceptions to this occurred in 2010 when the ecosystem remained a weaker than normal carbon sink into April due to a strong El Niño-related winter with an exceptionally deep snowpack (maximum snow depth = 123 cm), and in 2014 when the minimum snowpack was followed by a warm summer that diminished GPP more than  $R_{\text{eco}}$ . Throughout the nine year record (excluding low values in 2013 and 2014), the cumulative annual GPP varied by only  $\sim 100 \text{ g C m}^{-2}$  per year (Fig. 8b).

### 3.5. Controls on the seasonal carbon cycle

A proportional relationship between winter precipitation and warm season forest productivity has been established across a range of temperate mountain ecosystems (Trujillo et al., 2012; Knowles et al., 2018). A similar relationship was observed at Mt. Bigelow despite the seasonally variable snowpack and the relatively greater magnitude of summer precipitation (Fig. 9a). The importance of winter precipitation

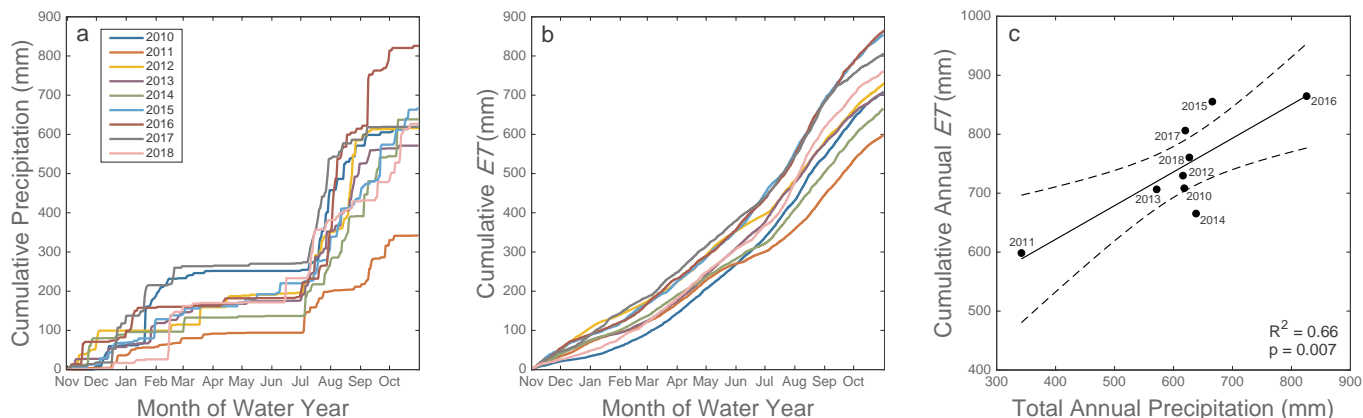


Fig. 7. Inter-annual hydrological variability and the relationship between precipitation and ET.

to warm season *wNEE* contrasts the monsoon-dependent carbon uptake patterns at lower elevations throughout the Southwest (Biederman et al., 2017), and demonstrates the importance of winter precipitation and spring snowmelt to subsurface recharge in sky island ecosystems (Dwivedi et al., 2019). The concept of snow aridity incorporates the temperature-dependent effects of snow precipitation fraction and atmospheric demand (*PET*) (Knowles et al., 2017). Snow aridity may thus function as a particularly sensitive indicator of ecosystem dynamics in areas that receive both snow and rain and may be subject to seasonal moisture limitation. Snow aridity, calculated as the quotient of the summed November to April *PET* and maximum snow depth, was in fact the best single predictor of the warm season carbon sink strength at Mt. Bigelow, and explained 86% of the variation in combined cumulative *NEE* during the pre-monsoon, monsoon, and fall (Fig. 9b). The unique outlier from this regression was WY 2015, which received the most temporally consistent (year-round) precipitation as evidenced by the shortest pre-monsoon dry period (Fig. 7a). In accord with carbon uptake during periods of favorable winter weather, air temperature was a good predictor of the winter *NEE* (Fig. 9c).

In order to gain a more complete understanding of the processes underlying net carbon cycling patterns, we investigated the seasonal temperature sensitivity of *GPP* and  $R_{eco}$  (Fig. 10). We observed contrasting temperature limitation to *GPP* during winter and the pre-monsoon as a function of moisture availability. Higher  $T_{air}$  during the winter was associated with fair weather and above-freezing conditions throughout the night that resulted in a positive correlation between air temperature and *GPP* (Fig. 10a). The exception to this was 2010 when *GPP* was curtailed due to a deep and long lasting snowpack. In contrast, high  $T_{air}$  during the pre-monsoon resulted in the annual *VPD* maximum

that exacerbated dry conditions (Fig. 10b); moisture limitation was alleviated with the onset of monsoon precipitation, resulting in a return to a positive relationship between  $T_{air}$  and *GPP* (Fig. 10c). From these results, we conclude that the seasonality of forecasted warming, and the degree to which reduced warm season *GPP* may be offset by increased winter *GPP* (e.g., Wolf et al., 2016), will be critical to future carbon cycling trends in montane sky island ecosystems.

Given that  $R_{eco}$  is comprised of both autotrophic and heterotrophic respiration, we evaluated temperature sensitivity using soil as opposed to air temperature. We observed similar trends between  $T_{soil}$  and  $R_{eco}$  at all measurement depths, but generally higher temperature sensitivity nearer to the surface (data not shown) in accord with increasing carbon substrate (Jobbágy and Jackson, 2000). Soil temperature was not a significant predictor of  $R_{eco}$  during the winter or the pre-monsoon. This was likely due to low and relatively stable  $R_{eco}$  fluxes during the winter (Figs. 5f and 6c), and the confounding and persistent influence of moisture limitation during the pre-monsoon, respectively (Sánchez-Cañete et al., 2018; Stielstra et al., 2015; Fig. 7a). The  $R_{eco}$  was much higher during the monsoon compared to any other time of year, and soil temperature was a significant predictor of monsoon  $R_{eco}$ . Lower than expected  $R_{eco}$  during the 2016 monsoon coincided with record precipitation that may have increased  $CO_2$  dissolution or silicate weathering within the soil profile (Olshansky et al., 2019), as has been shown during wet periods near the study site (Sánchez-Cañete et al., 2018).

4. Conclusion

The sky island montane forest on Mt. Bigelow has the potential for year-round productivity and thus represented a larger carbon sink than

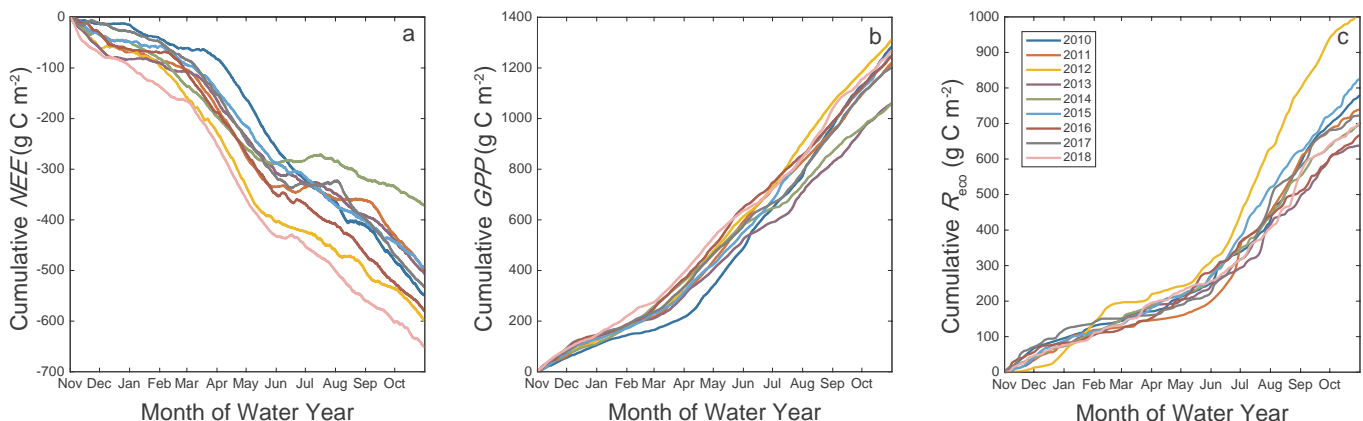


Fig. 8. Inter-annual carbon cycling variability.

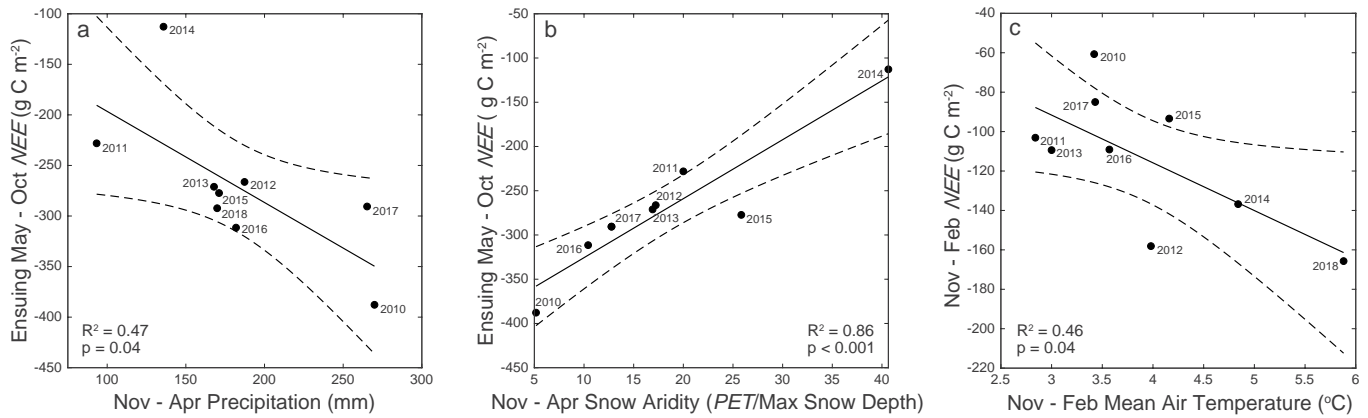


Fig. 9. Seasonal controls on the net ecosystem exchange of carbon dioxide (NEE).

colder, wetter montane forest ecosystems in the western USA. The magnitude of seasonal carbon fluxes varied with changes in temperature, precipitation amount and type, and aridity that resulted in temporal asynchrony between peak carbon inputs and outputs from the system. Consequently, maximum carbon sequestration occurred during the spring and fall when  $R_{eco}$  was low relative to  $GPP$ . Episodic moisture limitation was mainly restricted to the dry pre-monsoon period when forest activity depended on both the magnitude of antecedent moisture inputs and the timing of the monsoon rains. From that point,  $R_{eco}$  variability principally determined the carbon balance for the remainder of the year. A snow aridity metric that incorporated moisture supply (maximum snow depth) and demand (potential evapotranspiration)

was the best predictor of the integrated non-winter carbon balance.

Despite the location of the study site in the arid southwestern USA, the elevation and bimodal precipitation regime combined to promote favorable conditions to vegetation growth for most of the nine-year study period. This result suggests that sky island montane forests may be uniquely adapted to buffer forecasted drought and/or increased temperature relative to evergreen conifer forests that depend on winter precipitation to a greater degree. Considering the potential for environmental conditions at higher latitude forests to more closely resemble the current conditions at Mt. Bigelow, these results may also have a more widespread bearing on the response of more northerly forests to climate change. As such, we highlight the possibility for

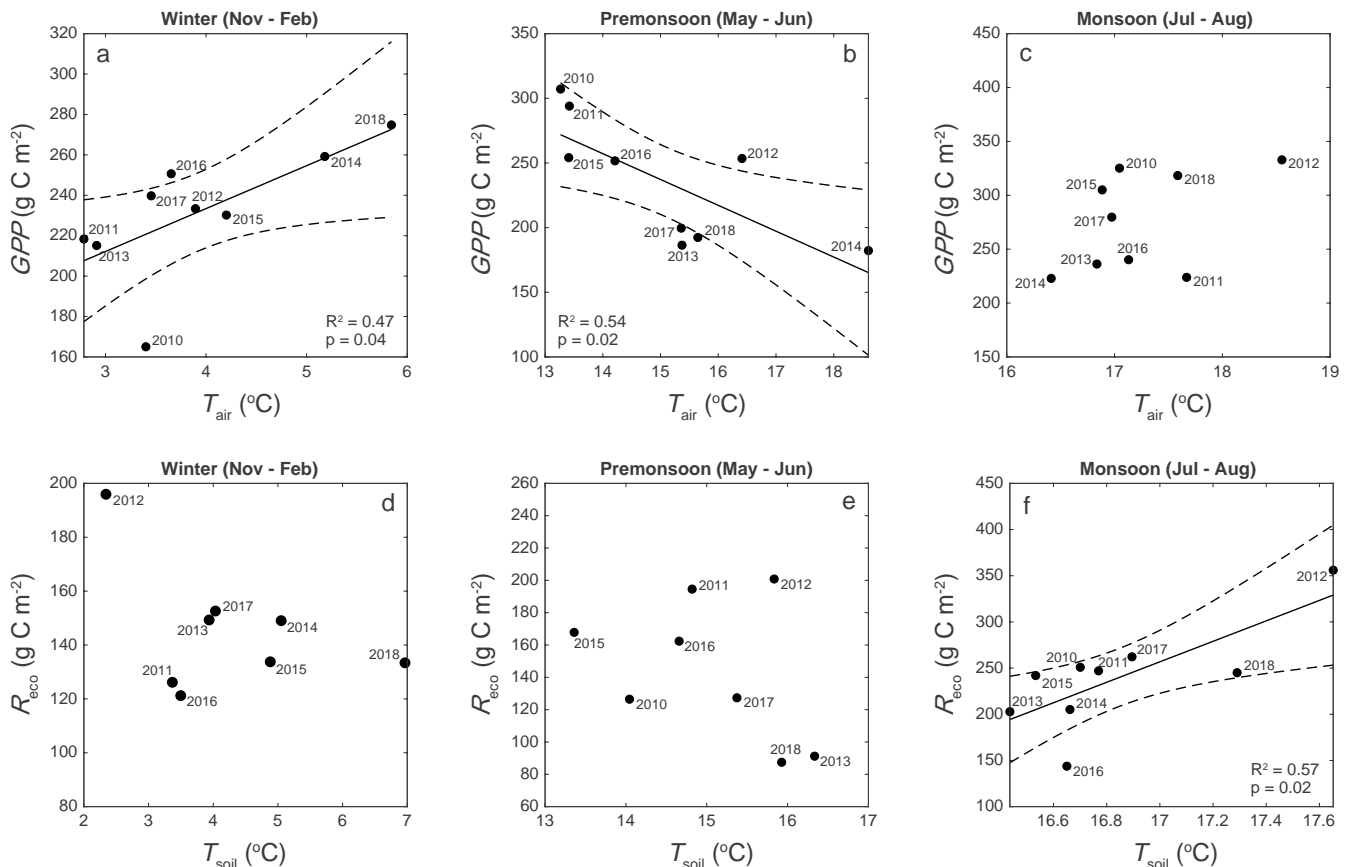


Fig. 10. The seasonal relationship between (a-c) air temperature ( $T_{air}$ ) and gross primary productivity ( $GPP$ ) and (d-f) soil temperature ( $T_{soil}$ ) and ecosystem respiration ( $R_{eco}$ ).

warming to increase forest activity during the shoulder seasons before and after winter, but also for warming and/or drying to intensify post-snowmelt moisture limitation, especially in areas where summer precipitation is scarce, or in the case of an increasingly delayed monsoon. Since the relative strength of these effects will ultimately determine the montane forest carbon sink throughout the western USA, future work to address this question quantitatively via synthetic observational or modeling analysis is especially warranted. In this way, measurements from climatically distinct locations such as sky islands can be leveraged to constrain the impact of higher temperatures or seasonal precipitation on carbon cycling throughout the montane forest biome.

### Declaration of Competing Interest

The authors declare that they have no known competing financial interests or personal relationships that could have appeared to influence the work reported in this paper.

### Acknowledgements

Funding for the Mt. Bigelow operation and maintenance was provided by National Science Foundation EAR awards 0724958 and 1331408 to the Catalina-Jemez Critical Zone Observatory. Funding for J.F.K. was provided by the U.S. Department of Energy's Office of Science. We thank R. Bryant (USDA-ARS) for help with Fig. 1 and acknowledge many graduate students and research technicians who have supported this work including Brian Chazar, Krystine Nelson, Patrick Murphy, Maggie Heard, Ashley Weide, and Evan Sommer. The Mt. Bigelow eddy covariance data are available from the AmeriFlux (site code US-MtB) data repository (<http://ameriflux.lbl.gov>); analysis codes for figures and tables are available upon request from the corresponding author. The authors declare no conflict of interest. USDA is an equal opportunity employer.

### References

- Adams, D.K., Comrie, A.C., 1997. The North American monsoon. *Bull. Am. Meteorol. Soc.* 78, 2197–2213. [https://doi.org/10.1175/1520-0477\(1997\)078<2197:TNAM>2.0.CO;2](https://doi.org/10.1175/1520-0477(1997)078<2197:TNAM>2.0.CO;2).
- Ahlstrom, A., Raupach, M.R., Schurgers, G., Smith, B., Arneeth, A., Jung, M., Reichstein, M., Canadell, J.G., Friedlingstein, P., Jain, A.K., Kato, E., Poulter, B., Sitch, S., Stocker, B.D., Viovy, N., Wang, Y.P., Wiltshire, A., Zaehle, S., Zeng, N., 2015. The dominant role of semi-arid ecosystems in the trend and variability of the land CO<sub>2</sub> sink. *Science* 348, 895–899. <https://doi.org/10.1126/science.aaa1668>.
- Ajami, H., Troch, P.A., Maddock, T., Meixner, T., Eastoe, C., 2011. Quantifying mountain block recharge by means of catchment-scale storage-discharge relationships. *Water Resour. Res.* 47. <https://doi.org/10.1029/2010WR009598>.
- Archer, S.R., Predick, K.I., 2008. Climate change and ecosystems of the southwestern United States. *Rangelands* 30, 23–28. [https://doi.org/10.2111/1551-501X\(2008\)30\[23:CCAEOT\]2.0.CO;2](https://doi.org/10.2111/1551-501X(2008)30[23:CCAEOT]2.0.CO;2).
- Baldocchi, D., 2008. "Breathing" of the terrestrial biosphere: lessons learned from a global network of carbon dioxide flux measurement systems. *Aust. J. Bot.* 56, 1. <https://doi.org/10.1071/BT07151>.
- Bales, R.C., Molotch, N.P., Painter, T.H., Dettinger, M.D., Rice, R., Dozier, J., 2006. Mountain hydrology of the western United States. *Water Resour. Res.* 42. <https://doi.org/10.1029/2005WR004387>.
- Barnard, D.M., Knowles, J.F., Barnard, H.R., Goulden, M.L., Hu, J., Litvak, M.E., Molotch, N.P., 2018. Reevaluating growing season length controls on net ecosystem production in evergreen conifer forests. *Sci. Rep.* 8. <https://doi.org/10.1038/s41598-018-36065-0>.
- Barron-Gafford, G.A., Scott, R.L., Jenerette, G.D., Huxman, T.E., 2011. The relative controls of temperature, soil moisture, and plant functional group on soil CO<sub>2</sub> efflux at diel, seasonal, and annual scales. *J. Geophys. Res.* 116. <https://doi.org/10.1029/2010JG001442>.
- Berkehammer, M., Stefanescu, I.C., Joiner, J., Anderson, L., 2017. High sensitivity of gross primary production in the Rocky Mountains to summer rain. *Geophys. Res. Lett.* 44, 3643–3652. <https://doi.org/10.1002/2016GL072495>.
- Biederman, J.A., Scott, R.L., Arnone III, J.A., Jasoni, R.L., Litvak, M.E., Moreo, M.T., Papuga, S.A., Ponce-Campos, G.E., Schreiner-McGraw, A.P., Vivoni, E.R., 2018. Shrubland carbon sink depends upon winter water availability in the warm deserts of North America. *Agric. For. Meteorol.* 249, 407–419. <https://doi.org/10.1016/j.agrformet.2017.11.005>.
- Biederman, J.A., Scott, R.L., Bell, T.W., Bowling, D.R., Dore, S., Garatuza-Payan, J., Kolb, T.E., Krishnan, P., Krofcheck, D.J., Litvak, M.E., Maurer, G.E., Meyers, T.P., Oechel, W.C., Papuga, S.A., Ponce-Campos, G.E., Rodriguez, J.C., Smith, W.K., Vargas, R., Watts, C.J., Yeepez, E.A., Goulden, M.L., 2017. CO<sub>2</sub> exchange and evapotranspiration across dryland ecosystems of southwestern North America. *Glob. Change Biol.* 23, 4204–4221. <https://doi.org/10.1111/gcb.13686>.
- Birch, H.F., 1958. The effect of soil drying on humus decomposition and nitrogen availability. *Plant Soil* 10, 9–31. <https://doi.org/10.1007/BF01343734>.
- Bourdeau, P.F., 1959. Seasonal variations of the photosynthetic efficiency of evergreen conifers. *Ecology* 40, 63–67. <https://doi.org/10.2307/1929923>.
- Breshears, D.D., Cobb, N.S., Rich, P.M., Price, K.P., Allen, C.D., Balice, R.G., Romme, W.H., Kastens, J.H., Floyd, M.L., Belnap, J., Anderson, J.J., Myers, O.B., Meyer, C.W., 2005. Regional vegetation die-off in response to global-change-type drought. *Proc. Natl. Acad. Sci.* 102, 15144–15148. <https://doi.org/10.1073/pnas.0505734102>.
- Brown-Mitic, C., Shuttleworth, W.J., Chawn Harlow, R., Petti, J., Burke, E., Bales, R., 2007. Seasonal water dynamics of a sky island subalpine forest in semi-arid southwestern United States. *J. Arid Environ.* 69, 237–258. <https://doi.org/10.1016/j.jaridenv.2006.09.005>.
- Burba, G., Schmidt, A., Scott, R.L., Nakai, T., Kathilankal, J., Fratini, G., Hanson, C., Law, B., McDermitt, D.K., Eckles, R., Furtaw, M., Velgersdyk, M., 2012. Calculating CO<sub>2</sub> and H<sub>2</sub>O eddy covariance fluxes from an enclosed gas analyzer using an instantaneous mixing ratio. *Glob. Change Biol.* 18, 385–399. <https://doi.org/10.1111/j.1365-2486.2011.02536.x>.
- Burba, G.G., McDermitt, D.K., Grelle, A., Anderson, D.J., Xu, L., 2008. Addressing the influence of instrument surface heat exchange on the measurements of CO<sub>2</sub> flux from open-path gas analyzers. *Glob. Change Biol.* 14, 1854–1876. <https://doi.org/10.1111/j.1365-2486.2008.01606.x>.
- Cayan, D.R., Redmond, K.T., Riddle, L.G., 1999. ENSO and hydrologic extremes in the western United States. *J. Clim.* 12, 2881–2893. [https://doi.org/10.1175/1520-0442\(1999\)012<2881:EAHETT>2.0.CO;2](https://doi.org/10.1175/1520-0442(1999)012<2881:EAHETT>2.0.CO;2).
- Chubb, T., Manton, M.J., Siems, S.T., Peace, A.D., Bilish, S.P., 2015. Estimation of wind-induced losses from a precipitation gauge network in the Australian snowy mountains. *J. Hydrometeorol.* 16, 2619–2638. <https://doi.org/10.1175/JHM-D-14-0216.1>.
- Churkina, G., Schimel, D., Braswell, B.H., Xiao, X., 2005. Spatial analysis of growing season length control over net ecosystem exchange. *Glob. Change Biol.* 11, 1777–1787. <https://doi.org/10.1111/j.1365-2486.2005.001012.x>.
- Cook, B.I., Ault, T.R., Smerdon, J.E., 2015. Unprecedented 21st century drought risk in the American southwest and central plains. *Sci. Adv.* 1, e1400082. <https://doi.org/10.1126/sciadv.1400082>.
- Cook, B.I., Seager, R., 2013. The response of the North American monsoon to increased greenhouse gas forcing. *J. Geophys. Res. Atmospheres* 118, 1690–1699. <https://doi.org/10.1002/jgrd.50111>.
- Dale, V.H., Joyce, L.A., McNulty, S., Neilson, R.P., Ayres, M.P., Flannigan, M.D., Hanson, P.J., Irland, L.C., Lugo, A.E., Peterson, C.J., Simberloff, D., Swanson, F.J., Stocks, B.J., Michael Wotton, B., 2001. Climate change and forest disturbances. *Bioscience* 51, 723–734. [https://doi.org/10.1641/0006-3568\(2001\)051\[0723:CCAFD\]2.0.CO;2](https://doi.org/10.1641/0006-3568(2001)051[0723:CCAFD]2.0.CO;2).
- De Roo, F., Zhang, S., Huq, S., Mauder, M., 2018. A semi-empirical model of the energy balance closure in the surface layer. *PLoS ONE* 13, e0209022. <https://doi.org/10.1371/journal.pone.0209022>.
- Desai, A.R., Moore, D.J.P., Ahue, W.K.M., Wilkes, P.T.V., De Wekker, S.F.J., Brooks, B.G., Campos, T.L., Stephens, B.B., Monson, R.K., Burns, S.P., Quaife, T., Aulenbach, S.M., Schimel, D.S., 2011. Seasonal pattern of regional carbon balance in the central Rocky Mountains from surface and airborne measurements. *J. Geophys. Res.* 116. <https://doi.org/10.1029/2011JG001655>.
- Dierauer, J.R., Allen, D.M., Whitfield, P.H., 2019. Snow drought risk and susceptibility in the western United States and southwestern Canada. *Water Resour. Res.* 55, 3076–3091. <https://doi.org/10.1029/2018WR023229>.
- Dore, S., Montes-Helu, M., Hart, S.C., Hungate, B.A., Koch, G.W., Moon, J.B., Finkral, A.J., Kolb, T.E., 2012. Recovery of ponderosa pine ecosystem carbon and water fluxes from thinning and stand-replacing fire. *Glob. Change Biol.* 18, 3171–3185. <https://doi.org/10.1111/j.1365-2486.2012.02775.x>.
- Douglas, M.W., Maddox, R.A., Howard, K., 1993. The Mexican monsoon. *J. Clim.* 6, 1665–1677.
- Dwivedi, R., Meixner, T., McIntosh, J.C., Ferré, P.A.T., Eastoe, C.J., Niu, G., Minor, R.L., Barron-Gafford, G.A., Chorover, J., 2019. Hydrologic functioning of the deep critical zone and contributions to streamflow in a high-elevation catchment: testing of multiple conceptual models. *Hydrol. Process.* 33, 476–494. <https://doi.org/10.1002/hyp.13363>.
- Foken, T., 2008. The energy balance closure problem: an overview. *Ecol. Appl.* 18, 1351–1367. <https://doi.org/10.1890/06-0922.1>.
- Goulden, M.L., Munger, J.W., Fan, S.-M., Daube, B.C., Wofsy, S.C., 1996. Measurements of carbon sequestration by long-term eddy covariance: methods and a critical evaluation of accuracy. *Glob. Change Biol.* 2, 169–182. <https://doi.org/10.1111/j.1365-2486.1996.tb00070.x>.
- Guan, K., Pan, M., Li, H., Wolf, A., Wu, J., Medvigy, D., Caylor, K.K., Sheffield, J., Wood, E.F., Malhi, Y., Liang, M., Kimball, J.S., Saleska, S.R., Berry, J., Joiner, J., Lyapustin, A.I., 2015. Photosynthetic seasonality of global tropical forests constrained by hydroclimate. *Nat. Geosci.* 8, 284–289. <https://doi.org/10.1038/ngeo2382>.
- Hamerlynck, E.P.L., Scott, R., Barron-Gafford, G.A., 2013. Consequences of cool-season drought-induced plant mortality to Chihuahuan desert grassland ecosystem and soil respiration dynamics. *Ecosystems* 16, 1178–1191. <https://doi.org/10.1007/s10021-013-9675-y>.
- Havranek, W., Tranquillini, W., 1995. Physiological processes during winter dormancy and their ecological significance. In: Smith, W.K., Hinckley, T.M. (Eds.), *Ecophysiology of Coniferous Forests*. Academic Press, San Diego, pp. 95–124.
- Higgins, R.W., Chen, Y., Douglas, A.V., 1999. Interannual variability of the North American warm season precipitation regime. *J. Clim.* 12, 653–680. [https://doi.org/10.1175/1520-0442\(1999\)012<0653:IVOTNA>2.0.CO;2](https://doi.org/10.1175/1520-0442(1999)012<0653:IVOTNA>2.0.CO;2).
- Hu, J., Moore, D.J.P., Burns, S.P., Monson, R.K., 2010. Longer growing seasons lead to less carbon sequestration by a subalpine forest. *Glob. Change Biol.* 16, 771–783. <https://doi.org/10.1111/j.1365-2486.2009.01967.x>.
- Huxman, T.E., Turnipseed, A.A., Sparks, J.P., Harley, P.C., Monson, R.K., 2003. Temperature as a control over ecosystem CO<sub>2</sub> fluxes in a high-elevation, subalpine forest. *Oecologia* 134, 537–546. <https://doi.org/10.1007/s00442-002-1131-1>.

- Jobbágy, E.G., Jackson, R.B., 2000. The vertical distribution of soil organic carbon and its relation to climate and vegetation. *Ecol. Appl.* 10, 423–436. [https://doi.org/10.1890/1051-0761\(2000\)010\[0423:TVDOSO\]2.0.CO;2](https://doi.org/10.1890/1051-0761(2000)010[0423:TVDOSO]2.0.CO;2).
- Kelly, A.E., Goulden, M.L., 2016. A montane Mediterranean climate supports year-round photosynthesis and high forest biomass. *Tree Physiol.* 36, 459–468. <https://doi.org/10.1093/treephys/tpv131>.
- Kljun, N., Calanca, P., Rotach, M.W., Schmid, H.P., 2015. A simple two-dimensional parameterisation for flux footprint prediction (FFP). *Geosci. Model Dev.* 8, 3695–3713. <https://doi.org/10.5194/gmd-8-3695-2015>.
- Knowles, J.F., Burns, S.P., Blanken, P.D., Monson, R.K., 2015. Fluxes of energy, water, and carbon dioxide from mountain ecosystems at Niwot Ridge, Colorado. *Plant Ecol. Divers.* 8, 663–676. <https://doi.org/10.1080/17550874.2014.904950>.
- Knowles, J.F., Lestak, L.R., Molotch, N.P., 2017. On the use of a snow aridity index to predict remotely sensed forest productivity in the presence of bark beetle disturbance. *Water Resour. Res.* 53, 4891–4906. <https://doi.org/10.1002/2016WR019887>.
- Knowles, J.F., Molotch, N.P., Trujillo, E., Litvak, M.E., 2018. Snowmelt-driven trade-offs between early and late season productivity negatively impact forest carbon uptake during drought. *Geophys. Res. Lett.* 45, 3087–3096. <https://doi.org/10.1002/2017GL076504>.
- Lasslop, G., Reichstein, M., Papale, D., Richardson, A.D., Arneth, A., Barr, A., Stoy, P., Wohlfahrt, G., 2010. Separation of net ecosystem exchange into assimilation and respiration using a light response curve approach: critical issues and global evaluation. *Glob. Change Biol.* 16, 187–208. <https://doi.org/10.1111/j.1365-2486.2009.02041.x>.
- Handbook of Micrometeorology: A Guide for Surface Flux Measurements and Analysis.** In: Lee, X., Massman, W., Law, B. (Eds.), *Handbook of Micrometeorology: A Guide for Surface Flux Measurements and Analysis*. Kluwer Academic Publishers, Dordrecht.
- Leung, L.R., Qian, Y., Bian, X., Hunt, A., 2003. Hydroclimate of the western United States based on observations and regional climate simulation of 1981–2000. Part II: mesoscale ENSO anomalies. *J. Clim.* 16, 1912–1928. [https://doi.org/10.1175/1520-0442\(2003\)016<1912:HOTWUS>2.0.CO;2](https://doi.org/10.1175/1520-0442(2003)016<1912:HOTWUS>2.0.CO;2).
- Ma, S., Baldocchi, D.D., Hatala, J.A., Detto, M., Curiel Yuste, J., 2012. Are rain-induced ecosystem respiration pulses enhanced by legacies of antecedent photodegradation in semi-arid environments? *Agric. For. Meteorol.* 154–155, 203–213. <https://doi.org/10.1016/j.agrformet.2011.11.007>.
- Meisner, A., Rousk, J., Bååth, E., 2015. Prolonged drought changes the bacterial growth response to rewetting. *Soil Biol. Biochem.* 88, 314–322. <https://doi.org/10.1016/j.soilbio.2015.06.002>.
- Mote, P.W., Li, S., Lettenmaier, D.P., Xiao, M., Engel, R., 2018. Dramatic declines in snowpack in the western US. *Npj Clim. Atmospheric Sci.* 1. <https://doi.org/10.1038/s41612-018-0012-1>.
- Novick, K., Brantley, S., Miniati, C.F., Walker, J., Vose, J.M., 2014. Inferring the contribution of advection to total ecosystem scalar fluxes over a tall forest in complex terrain. *Agric. For. Meteorol.* 185, 1–13. <https://doi.org/10.1016/j.agrformet.2013.10.010>.
- Novick, K.A., Ficklin, D.L., Stoy, P.C., Williams, C.A., Bohrer, G., Oishi, A.C., Papuga, S.A., Blanken, P.D., Noormets, A., Sulman, B.N., Scott, R.L., Wang, L., Phillips, R.P., 2016. The increasing importance of atmospheric demand for ecosystem water and carbon fluxes. *Nat. Clim. Change* 6, 1023–1027. <https://doi.org/10.1038/nclimate3114>.
- Noy-Meir, I., 1973. Desert ecosystems: environment and producers. *Annu. Rev. Ecol. Syst.* 4, 25–51. <https://doi.org/10.1146/annurev.es.04.110173.000325>.
- Olshansky, Y., Knowles, J.F., Barron-Gafford, G.A., Rasmussen, C., Abramson, N., Chorover, J., 2019. Soil fluid biogeochemical response to climatic events. *J. Geophys. Res. Biogeosci.* 124. <https://doi.org/10.1029/2019JG005216>.
- Pascale, S., Carvalho, L.M., Adams, D.K., Castro, C.L., Cavalcanti, I.F.A., 2019. Current and future variations of the monsoons of the Americas in a warming climate. *Curr. Clim. Change Rep.* 5, 125–144. <https://doi.org/10.1007/s40641-019-00135-w>.
- Peltier, D.M.P., Ogle, K., 2019. Legacies of La Niña: North American monsoon can rescue trees from winter drought. *Glob. Change Biol.* 25, 121–133. <https://doi.org/10.1111/gcb.14487>.
- Piao, S., Friedlingstein, P., Ciais, P., Viovy, N., Demarty, J., 2007. Growing season extension and its impact on terrestrial carbon cycle in the Northern Hemisphere over the past 2 decades. *Glob. Biogeochem. Cycles* 21, 1–11. <https://doi.org/10.1029/2006GB002888>.
- Potts, D.L., Minor, R.L., Braun, Z., Barron-Gafford, G.A., 2017. Photosynthetic phenological variation may promote coexistence among co-dominant tree species in a Madrean sky island mixed conifer forest. *Tree Physiol.* 37, 1229–1238. <https://doi.org/10.1093/treephys/tpx076>.
- Rungee, J., Bales, R., Goulden, M., 2018. Evapotranspiration response to multiyear dry periods in the semiarid western United States. *Hydrol. Process.* <https://doi.org/10.1002/hyp.13322>.
- Saleska, S.R., Miller, S.D., Matross, D.M., Goulden, M.L., Wofsy, S.C., da Rocha, H.R., de Camargo, P.B., Crill, P., Daube, B.C., de Freitas, H.C., Hutyrá, L., Keller, M., Kirchhoff, V., Menton, M., Munger, J.W., Pyle, E.H., Rice, A.H., Silva, H., 2003. Carbon in amazon forests: unexpected seasonal fluxes and disturbance-induced losses. *Science* 302, 1554–1557. <https://doi.org/10.1126/science.1091165>.
- Sánchez-Cañete, E.P., Barron-Gafford, G.A., Chorover, J., 2018. A considerable fraction of soil-respired CO<sub>2</sub> is not emitted directly to the atmosphere. *Sci. Rep.* 8. <https://doi.org/10.1038/s41598-018-29803-x>.
- Schimel, D., Kittel, T.G.F., Running, S., Monson, R., Turnipseed, A., Anderson, D., 2002. Carbon sequestration studied in western U.S. mountains. *Eos Trans. Am. Geophys. Union* 83, 445. <https://doi.org/10.1029/2002EO000314>.
- Schwalm, C.R., Williams, C.A., Schaefer, K., Baldocchi, D., Black, T.A., Goldstein, A.H., Law, B.E., Oechel, W.C., Paw U, K.T., Scott, R.L., 2012. Reduction in carbon uptake during turn of the century drought in western North America. *Nat. Geosci.* 5, 551–556. <https://doi.org/10.1038/ngeo1529>.
- Scott, R.L., Biederman, J.A., Hamerlynck, E.P., Barron-Gafford, G.A., 2015. The carbon balance pivot point of southwestern U.S. semiarid ecosystems: insights from the 21st century drought. *J. Geophys. Res. Biogeosci.* 120, 2612–2624. <https://doi.org/10.1002/2015JG003181>.
- Scott, R.L., Hamerlynck, E.P., Jenerette, G.D., Moran, M.S., Barron-Gafford, G.A., 2010. Carbon dioxide exchange in a semidesert grassland through drought-induced vegetation change. *J. Geophys. Res.* 115. <https://doi.org/10.1029/2010JG001348>.
- Scott, R.L., Huxman, T.E., Barron-Gafford, G.A., Jenerette, G.D., Young, J.M., Hamerlynck, E.P., 2014. When vegetation change alters ecosystem water availability. *Glob. Change Biol.* 20, 2198–2210. <https://doi.org/10.1111/gcb.12511>.
- Scott, R.L., Jenerette, G.D., Potts, D.L., Huxman, T.E., 2009. Effects of seasonal drought on net carbon dioxide exchange from a woody-plant-encroached semiarid grassland. *J. Geophys. Res.* 114. <https://doi.org/10.1029/2008JG000900>.
- Seager, R., Ting, M., Held, I., Kushnir, Y., Lu, J., Vecchi, G., Huang, H.-P., Harnik, N., Leetmaa, A., Lau, N.-C., Li, C., Velez, J., Naik, N., 2007. Model projections of an imminent transition to a more arid climate in southwestern North America. *Science* 316, 1181–1184. <https://doi.org/10.1126/science.1139601>.
- Shuttleworth, J.W., 1993. *Evaporation. In: Maidment, D.R. (Ed.), Handbook of Hydrology*. McGraw-Hill, New York, pp. 4.1–4.53.
- Smith, A.P., Bond-Lamberty, B., Benscoter, B.W., Tfaily, M.M., Hinkle, C.R., Liu, C., Bailey, V.L., 2017. Shifts in pore connectivity from precipitation versus groundwater rewetting increases soil carbon loss after drought. *Nat. Commun.* 8. <https://doi.org/10.1038/s41467-017-01320-x>.
- Stielstra, C.M., Lohse, K.A., Chorover, J., McIntosh, J.C., Barron-Gafford, G.A., Perdrial, J.N., Litvak, M., Barnard, H.R., Brooks, P.D., 2015. Climatic and landscape influences on soil moisture are primary determinants of soil carbon fluxes in seasonally snow-covered forest ecosystems. *Biogeochemistry* 123, 447–465. <https://doi.org/10.1007/s10533-015-0078-3>.
- Stiperski, I., Rotach, M.W., 2016. On the measurement of turbulence over complex mountain terrain. *Bound.-Layer Meteorol.* 159, 97–121. <https://doi.org/10.1007/s10546-015-0103-z>.
- Szejner, P., Wright, W.E., Babst, F., Belmecheri, S., Trouet, V., Leavitt, S.W., Ehleringer, J.R., Monson, R.K., 2016. Latitudinal gradients in tree ring stable carbon and oxygen isotopes reveal differential climate influences of the North American monsoon system: intra-annual Tree Ring C and O isotopes. *J. Geophys. Res. Biogeosci.* 121, 1978–1991. <https://doi.org/10.1002/2016JG003460>.
- Thomas, B., Behrangi, A., Famiglietti, J., 2016. Precipitation intensity effects on groundwater recharge in the southwestern United States. *Water (Basel)* 8, 90. <https://doi.org/10.3390/w8030090>.
- Trujillo, E., Molotch, N.P., Goulden, M.L., Kelly, A.E., Bales, R.C., 2012. Elevation-dependent influence of snow accumulation on forest greening. *Nat. Geosci.* 5, 705–709. <https://doi.org/10.1038/ngeo1571>.
- Turnipseed, A.A., Blanken, P.D., Anderson, D.E., Monson, R.K., 2002. Energy budget above a high-elevation subalpine forest in complex topography. *Agric. For. Meteorol.* 110, 177–201. [https://doi.org/10.1016/S0168-1923\(01\)00290-8](https://doi.org/10.1016/S0168-1923(01)00290-8).
- Udall, B., Overpeck, J., 2017. The twenty-first century Colorado River hot drought and implications for the future. *Water Resour. Res.* 53, 2404–2418. <https://doi.org/10.1002/2016WR019638>.
- Valentini, R., Matteucci, G., Dolman, A.J., Schulze, E.-D., Rebmann, C., Moors, E.J., Granier, A., Gross, P., Jensen, N.O., Pilegaard, K., Lindroth, A., Grelle, A., Bernhofer, C., Grünwald, T., Aubinet, M., Ceulemans, R., Kowalski, A.S., Vesala, T., Rannik, Ü., Berbigier, P., Loustau, D., Guðmundsson, J., Thorgeirsson, H., Ibrom, A., Morgenstern, K., Clement, R., Moncrieff, J., Montagnani, L., Minerbi, S., Jarvis, P.G., 2000. Respiration as the main determinant of carbon balance in European forests. *Nature* 404, 861–865. <https://doi.org/10.1038/35009084>.
- Warshall, P., 1995. The Madrean sky island archipelago: a planetary overview (No. RM-GTR-264). *Biodiversity and Management of the Madrean Archipelago: The Sky Islands of Southwestern United States and Northwestern Mexico*. U.S. Department of Agriculture, Forest Service, Rocky Mountain Forest and Range Experiment Station, Ft. Collins, CO. <https://doi.org/10.2737/RM-GTR-264>.
- Webb, E.K., Pearman, G.I., Leuning, R., 1980. Correction of flux measurements for density effects due to heat and water vapour transfer. *Q. J. R. Meteorol. Soc.* 106, 85–100. <https://doi.org/10.1002/qj.49710644707>.
- Williams, A.P., Allen, C.D., Millar, C.I., Swetnam, T.W., Michaelsen, J., Still, C.J., Leavitt, S.W., 2010. Forest responses to increasing aridity and warmth in the southwestern United States. *Proc. Natl. Acad. Sci.* 107, 21289–21294. <https://doi.org/10.1073/pnas.0914211107>.
- Wilson, K., Goldstein, A., Falge, E., Aubinet, M., Baldocchi, D., Berbigier, P., Bernhofer, C., Ceulemans, R., Dolman, H., Field, C., Grelle, A., Ibrom, A., Law, B.E., Kowalski, A., Meyers, T., Moncrieff, J., Monson, R., Oechel, W., Tenhunen, J., Valentini, R., Verma, S., 2002. Energy balance closure at FLUXNET sites. *Agric. For. Meteorol.* 113, 223–242. [https://doi.org/10.1016/S0168-1923\(02\)00109-0](https://doi.org/10.1016/S0168-1923(02)00109-0).
- Winchell, T.S., Barnard, D.M., Monson, R.K., Burns, S.P., Molotch, N.P., 2016. Earlier snowmelt reduces atmospheric carbon uptake in midlatitude subalpine forests. *Geophys. Res. Lett.* 43, 8160–8168. <https://doi.org/10.1002/2016GL069769>.
- Wolf, S., Keenan, T.F., Fisher, J.B., Baldocchi, D.D., Desai, A.R., Richardson, A.D., Scott, R.L., Law, B.E., Litvak, M.E., Brunsell, N.A., Peters, W., van der Laan-Luijckx, I.T., 2016. Warm spring reduced carbon cycle impact of the 2012 US summer drought. *Proc. Natl. Acad. Sci.* 113, 5880–5885. <https://doi.org/10.1073/pnas.1519620113>.
- Woodhouse, C.A., Meko, D.M., MacDonald, G.M., Stahle, D.W., Cook, E.R., 2010. A 1,200-year perspective of 21st century drought in southwestern North America. *Proc. Natl. Acad. Sci.* 107, 21283–21288. <https://doi.org/10.1073/pnas.0911197107>.
- Wutzler, T., Lucas-Moffat, A., Migliavacca, M., Knauer, J., Sichel, K., Šigut, L., Menzer, O., Reichstein, M., 2018. Basic and extensible post-processing of eddy covariance flux data with REddyProc. *Biogeosciences* 15, 5015–5030. <https://doi.org/10.5194/bg-15-5015-2018>.